

Transport Properties Governed by the Inductance of the Edges in $\text{Bi}_2\text{Sr}_2\text{CaCu}_2\text{O}_8$

H. Beidenkopf,^{1,*} Y. Myasoedov,¹ E. Zeldov,¹ E.H. Brandt,²
G.P. Mikitik,^{2,3} T. Tamegai,⁴ T. Sasagawa,⁵ and C. J. van der Beek⁶

¹Department of Condensed Matter Physics, Weizmann Institute of Science, Rehovot 76100, Israel

²Max-Planck-Institut für Metallforschung, Heisenbergstr. 3, D-70506 Stuttgart, Germany

³B. Verkin Institute for Low temperature Physics & Engineering, Kharkov 61103, Ukraine

⁴Department of Applied Physics, The University of Tokyo, Hongo, Bunkyo-ku, Tokyo 113-8656, Japan

⁵Materials and Structures Laboratory, Tokyo Institute of Technology, Kanagawa 226-8503, Japan

⁶Laboratoire des Solides Irradiées, CNRS UMR 7642 & CEA/IRAMIS/DRECAM,
Ecole Polytechnique, 91128 Palaiseau cedex, France

(Dated: December 4, 2018)

We study the distribution of transport current across superconducting $\text{Bi}_2\text{Sr}_2\text{CaCu}_2\text{O}_8$ crystals and the vortex flow through the sample edges. We show that the T_x transition is of electrodynamic rather than thermodynamic nature, below which vortex dynamics is governed by the edge inductance instead of the resistance. This allows measurement of the resistance down to two orders of magnitude below the transport noise. By irradiating the current contacts the resistive step at vortex melting is shown to be due to loss of c-axis correlations rather than breakdown of quasi-long-range order within the a-b planes.

PACS numbers: 74.25.Dw, 74.25.Bt, 74.25.Fy, 74.72.Hs

Numerous phase transitions have been proposed to interpret the intricate $B - T$ phase diagram of vortex matter in the high temperature superconductor $\text{Bi}_2\text{Sr}_2\text{CaCu}_2\text{O}_8$ (BSCCO) [1, 2]. The first-order melting at T_m , that separates a quasi-ordered vortex solid from a vortex liquid, is widely accepted to be a genuine thermodynamic phase transition [3, 4]. Experiments indicate that the glass line, T_g , is another thermodynamic transition that apparently separates amorphous solid from liquid at high fields [5, 6, 7, 8] and Bragg glass from depinned lattice at low fields [7, 8]. On the other hand, the T_x transition, which resides above T_m and T_g , has remained highly controversial. A number of experiments [9, 10, 11, 12, 13, 14], numerical simulations [15, 16], and theoretical studies [17, 18] argued that it is a transition into a phase with intermediate degree of order such as a disentangled liquid [19] or a decoupled- [20, 21], soft- [22], or super-solid [23, 24]. In this letter we show that T_x does not represent a thermodynamic transformation of a bulk vortex property, but rather reflects an *electrodynamic* crossover in the dynamic response of the sample *edges*. The inductance of the sample edges, though immeasurably low, completely governs the vortex dynamics below T_x . We use this finding to investigate the resistance due to vortex motion down to two orders of magnitude below the sensitivity of transport measurements.

The resistance of several BSCCO single crystals of typical size $1500 \times 350 \times 20 \mu\text{m}^3$ in a dc magnetic field, $H_{dc} \parallel c$ -axis, was measured using two complimentary techniques: directly via transport and indirectly by determining the ac current distribution with Biot-Savart law from the self-induced ac magnetic field profile using an array of $10 \times 10 \mu\text{m}^2$ GaAs Hall sensors. In addition, to eliminate the c-axis contribution to the measured resistance we irradiate

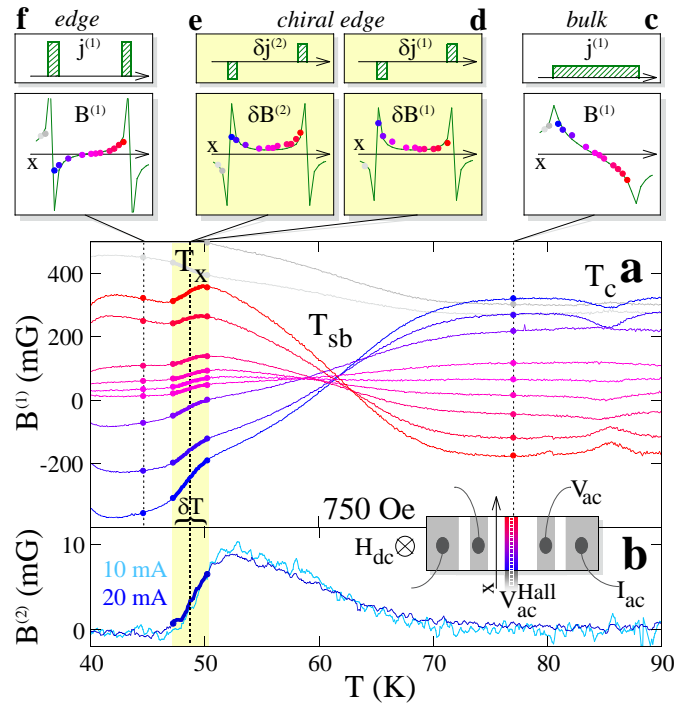


FIG. 1: (color online) Hall sensor array measurement of the ac magnetic field self-induced by a 15 mA, 73 Hz ac current in BSCCO crystal A. (a) First-harmonics of individual sensors. (b) Second-harmonics from a sensor close to the edge at two current amplitudes normalized to 10 mA. (c-f) Magnetic profiles measured (\bullet) and calculated (solid lines) from current profiles (upper panels) using the Biot-Savart law: (c) Uniform bulk flow at high temperatures turns to (f) edge flow at low temperatures. Chiral edge flow vanishes at T_x from (d) first- and (e) second-harmonics. Inset in (b): Schematic location of Hall sensors relative to the contacted sample.

ated the current contacts at GANIL (Caen, France) with 1 GeV Pb ions to a matching dose of $B_\Phi = 0.5$ T, while masking the rest of the sample, which remained pristine.

Figure 1(a) shows the temperature dependence of the current-induced ac field, $B^{(1)}(x)$. At high temperatures the current distributes uniformly because it is solely dictated by the flux flow resistance in the bulk, $R_b(T)$. Accordingly, $B^{(1)}(x)$ measured by the Hall sensors across the sample (Fig. 1(c), circles) fits perfectly to that calculated via Biot-Savart law (solid line) from a uniform current $j^{(1)}(x)$ (upper panel).

With cooling $B^{(1)}(x)$ gradually flattens out, becomes completely flat at T_{sb} , and eventually inverted at yet lower temperatures. The inverted $B^{(1)}(x)$ profile is associated with essentially pure edge currents (Fig. 1(f)). The Bean-Livingston surface barrier [25] and the platelet sample geometry [26] impose an energetic barrier that progressively impedes vortex passage through the edges. This defines an effective edge resistance, $R_e(T)$, that decreases rapidly with cooling and becomes smaller than the bulk resistance $R_b(T)$ below T_{sb} . As a result, most of the current shifts from the bulk, where little force is required to move vortices across, towards the edges, where it facilitates the hindered vortex entry and exit [27]. Bulk vortex pinning becomes dominant only at significantly lower temperature (not shown).

The dynamic properties of the surface barriers have two types of asymmetries. The first arises from the two edges of the sample generally having somewhat different microscopic imperfections. It leads to different edge resistances and therefore asymmetric current distribution between the right and left edges. The T_x line, situated below T_{sb} (Fig. 2), marks the temperature below which this right-left asymmetry sharply disappears and the amplitudes of the two edge currents become equal (Fig. 1(f)). Hence, an antisymmetric current component $\delta j^{(1)}$ (Fig. 1(d)), that was present above T_x , and its induced small symmetric contribution $\delta B^{(1)}(x) = B^{(1)}(x, T_x + \frac{\delta T}{2}) - B^{(1)}(x, T_x - \frac{\delta T}{2})$ to the otherwise antisymmetric $B^{(1)}(x)$, vanish below T_x .

The second type of asymmetry arises from the inherent asymmetry between hard vortex entry and easy exit through the surface barriers [28]. Since the vortex entry and exit sides swap during the ac cycle, this asymmetry gives rise to a unique chiral second harmonic edge current, $\delta j^{(2)}$, and to the corresponding second harmonic signal $\delta B^{(2)}(x)$ (Fig. 1(e)). It builds up gradually upon cooling (Fig. 1(b)) until it pinches off sharply at T_x (hereinafter determined at half of the $B^{(2)}(x)$ roll-off). Accordingly, T_x marks the temperature below which the vortex flow turns insensitive to both the entry-exit and the right-left asymmetries of the surface barriers.

The T_x transition was previously ascribed to the advent of a new vortex phase with a higher degree of order [9, 15, 16, 17, 18]. We show that T_x has rather electrodynamic nature, arising from the sample edges induc-

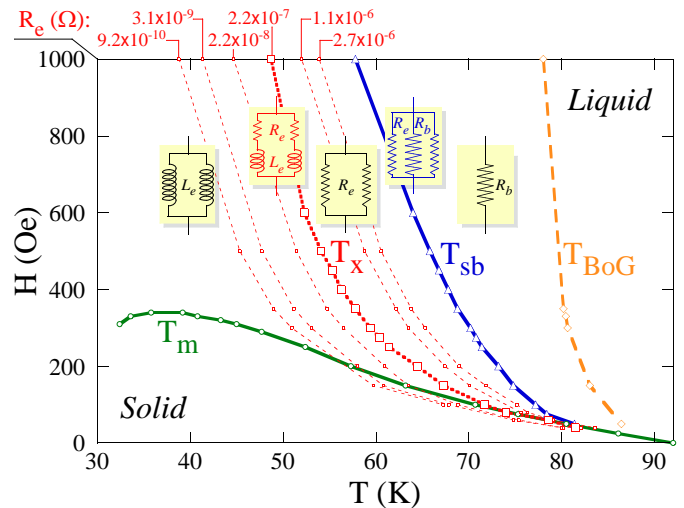


FIG. 2: (color online) High temperature phase diagram of the vortex matter in BSCCO crystal B. T_m is the first-order melting (\circ). Below T_{sb} (Δ) the edges shunt most of the current from the bulk, while below the frequency dependent T_x (\square) the edge impedance becomes predominantly inductive. Ion irradiated regions exhibit the Bose Glass transition, T_{BoG} (\diamond), below which vortices are pinned to columnar defects. The dotted lines represent equal edge-resistance contours extracted from the frequency and field dependence of T_x .

tance. Following Ref. [29] we model the vortex dynamics by equivalent electric circuit with three parallel channels - the bulk and two edges. Our measurements show no dependence on the current magnitude (Fig. 1(b), dark vs. pale lines). Therefore, we follow the Ohmic model of Ref. [29] that assigns each channel geometrical self and mutual inductances in series to their resistances.

The sample inductance is usually disregarded since it is immeasurably small in direct transport measurements. Nevertheless, it affects the current distribution in the sample. The effective edge inductance, as opposed to the edge resistance, is temperature independent and dictated solely by the geometry of the edges $L_e = (\mu_0/4\pi)l[\ln(2w/d) + 1/4]$, where l , w , and d are the sample's length, width, and thickness, respectively [29]. T_x is the temperature below which the edge impedance turns from being predominantly resistive to inductive, $R_e(T_x) = 2\pi f L_e$. Consequently, T_x is frequency dependent and allows sensitive determination of $R_e(T)$ similar to the extraction of resistance from ac susceptibility [30, 31]. At 350 Oe and $f = 73$ Hz we measure $T_x \simeq 59$ K. Using $L_e = 304$ pH, calculated from sample geometry, we obtain $R_e(59 \text{ K}) = 1.4 \times 10^{-7} \Omega$ (Fig. 3, white cross). Note, that this value is 2-3 orders of magnitude lower than the current dependent resistance measured simultaneously in transport (open circles), which below T_{sb} should reflect the edge resistance R_e .

The transport resistance measured in the geometry of Fig. 3(a), however, has a large contribution from the c-

axis resistivity, ρ_c . Due to the extreme anisotropy of BSCCO ρ_c is orders of magnitude larger than ρ_{ab} , giving rise to nonlinearities and shear effects [32, 33]. The dissipation due to ρ_c that arises from current tunneling between the CuO_2 planes, however, is not accounted in the electrodynamic considerations of the edge inductance [29]. The non-uniformity of current flow along the c -axis can be remedied by introducing columnar defects solely under the current contacts (see Fig. 3(b)). Below the Bose-glass transition, T_{BoG} (Fig. 2, diamonds), the vortices become strongly pinned to the columnar defects increasing the c -axis correlations and greatly reducing the sample anisotropy [34, 35, 36]. This is remarkably demonstrated in a multi-contact measurement of a sample irradiated in such a manner (Fig. 3(c)). Above T_{BoG} the high anisotropy results in poor c -axis current penetration. Therefore, the primary resistance, R_p , measured on the current injecting surface, is much higher than the secondary resistance, R_s , measured on the opposite surface. At T_{BoG} , signaled by the plunging c -axis resistance R_c , the secondary resistance recovers and equals the primary [37, 38]. After current contact irradiation the resistance, measured by voltage contacts in the central pristine region of the sample (Fig. 3, open squares), decreases by two orders of magnitude, and turns Ohmic. Moreover, the resistive behavior now becomes fully consistent with the inductive edge model. As shown below, all the data sets can be fitted by a single parameter - an effective edge inductance of $L_e = 490$ pH (black cross in Fig. 3). The similarity of this value to the calculated 304 pH is remarkable, considering the crude modeling of the edges (round wires of diameter d [29]) and the uncertainties in various parameters.

To further establish the role of the edge inductance in the T_x transition we extract $R_e(T, H)$ by repeatedly monitoring the current distribution with frequencies ranging from 0.3 Hz to 1 kHz. At all frequencies $B^{(2)}$ rises gradually with cooling (Fig. 4(a)), as more current is shunted to the edges, until it vanishes at a frequency-dependent temperature, $T_x(f)$. The extracted edge resistance, $2\pi f L_e$ versus $T_x(f, H)$ (Fig. 4(b), circles), matches accurately the resistance measured in transport (thin lines), and extrapolates it well below the transport noise floor. A fit to an Arrhenius behavior (dotted line) yields an edge energy barrier $U_e^o \sim 18T_c$.

The excellent agreement of the edge resistance extracted from $T_x(f)$ to that measured in transport confirms that the edge inductance drives the electrodynamic T_x transition. In terms of vortex dynamics, the resistive component of the edge impedance arises from vortex dissipation thermally activated over the surface barriers. Dissipation due to bulk vortex motion is negligible, since bulk pinning is very weak, hence $R_b \gg R_e$. Nevertheless, bulk redistribution of vortices reflects the inductive component of the edge impedance. With changing current polarity during the ac cycle the vortices, complying

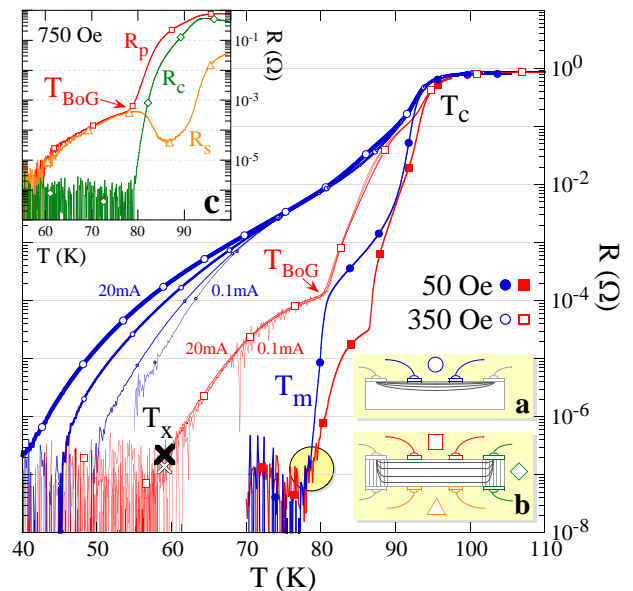


FIG. 3: (color online) The pristine transport resistance (BSCCO crystal B) is non-Ohmic (shrinking \circ : $I_{ac} = 20, 5, 1, 0.1$ mA, 73 Hz) due to non-uniform current flow along c -axis (inset a). After contact irradiation (\square) and below T_{BoG} as the current penetrates uniformly (inset b) the resistance turns Ohmic and matches that extracted from T_x (\times). Below the resistive step at T_m the pristine (\bullet) and irradiated (\blacksquare) resistances are equal. Inset c: Multi-contact measurement of a current-contact-irradiated sample (b). At low fields and below T_{BoG} , signaled by the vanishing c -axis resistance (\diamond), current distributes uniformly across the sample thickness, and the secondary resistance (Δ) equals the primary one (\square).

with the $B^{(1)}(x)$ profile of Fig. 1(f), shift from one side of the sample to the opposite in association with an inductive dB/dt . At high temperatures the number of vortices redistributing from right to left during half a cycle due to $dB^{(1)}(x)/dt$ is still much smaller than those that dissipatively cross the edges and move across the sample. With cooling, however, the number of vortices that cross the edges decreases exponentially. Below T_x it becomes negligible compared to the number of redistributing vortices. The second harmonic vanishes because vortex redistribution in a ‘closed box’ is necessarily antisymmetric. Our main finding is that although the edge inductance is immeasurably small in transport measurements, it completely governs vortex dynamics below T_x .

We now focus on the behavior of the edge resistance at melting. In the pristine sample a sharp resistive drop [39] is observed at T_m (Fig. 3, solid dots), whereas after contact irradiation the behavior is continuous (solid squares). Moreover, the two curves merge at the lowest measurable resistance (circled), indicating that in the presence of a uniform c -axis current the edge resistance shows no sharp features. Hence, the common resistive melting drop in BSCCO arises from a sharp drop in ρ_c .

Another intriguing feature at melting (Fig. 4(c), as-

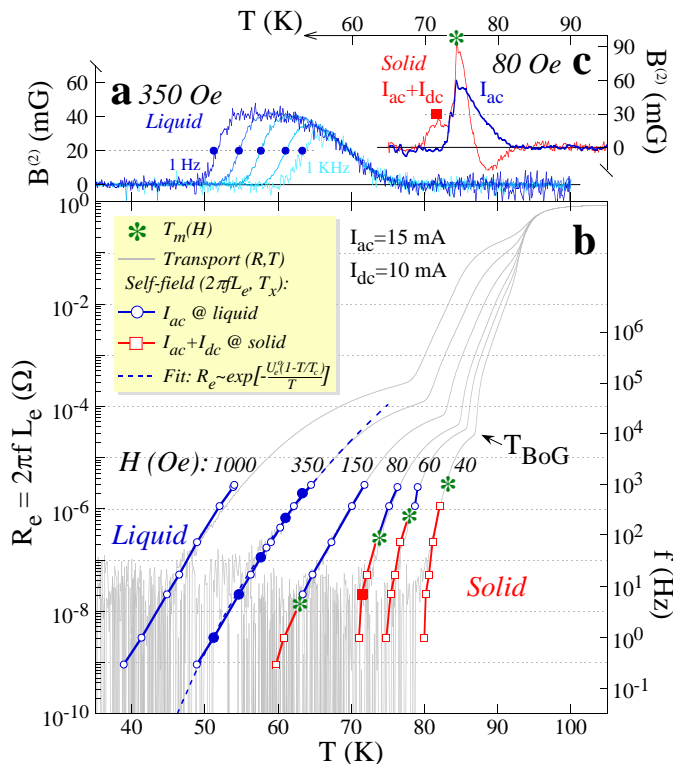


FIG. 4: (color online) (a) Second-harmonic signals showing the frequency dependence of T_x (\bullet). (b) It enables to extract the temperature dependent edge resistance (\circ) which is thermally activated (dashed) and accurately matches the measured transport resistance (thin lines). Below melting ($*$) a small dc bias is required to extract the edge resistance (\square). (c) This is seen in the second-harmonic signal (thick line) that vanishes at melting ($*$) but recovers with bias (thin line) before vanishing again at T_x (\blacksquare).

terisk) is a concurrent vanishing of $B^{(2)}$ (thick line). A more detailed analysis shows that this does not result from edge inductance, but reflects an increased surface barriers in the vortex solid due to enhanced c -axis correlations [28], which enhances the current flow symmetry. To break this enhanced symmetry below T_m and probe the edge inductance we add a small dc current bias. In its presence a finite second harmonic signal (Fig. 4(c), thin line) subsists below melting before vanishing at T_x (square). The detection of T_x below melting allows to extract the edge resistance within the solid phase (Fig. 4(b), squares), which fits perfectly and extrapolates the transport resistance. Consequently, we find that the edge resistance measured either in transport or by the edge inductance at T_x shows no pronounced feature at melting once the c -axis contribution is removed by current contact irradiation. This suggests that in highly anisotropic materials, such as BSCCO, the reported resistive melting step originates mostly from the loss of c -axis correlations through a simultaneous sublimation into a pancake gas [20, 40, 41]. In contrast, the loss of inter-vortex correla-

tions within the a - b planes at melting has no significant mark in the vortex flow rate through the edges.

Finally, our complete set of data is given by dotted lines in Fig. 2 that represent contours of equal edge resistance (*i.e.* measured at the same frequency) spanning three and a half orders of magnitude in the $H - T$ phase diagram. It is evident that the exponential temperature dependence of the edge resistance becomes steeper on approaching the melting as the contour lines bunch together. This is attributed to the enhanced stiffness of the pancake vortex stacks. Nevertheless, we do not find a singular behavior at melting which would have manifested itself in overlapping contour lines. On the contrary, once the c -axis contribution is eliminated the edge resistance in solid joins smoothly that of the liquid.

In summary, the spatial distribution of transport current and its frequency dependence show that the T_x line, tentatively ascribed to a phase transition of vortex matter in BSCCO, is rather an electrodynamic transition. Consequently, in the wide field and temperature range that lies below the T_x line the inductance of the sample edges, usually dismissed in transport experiments, dominates the current flow and causes ac displacement of vortices across the bulk without crossing the sample edges. At T_x , the inductive part of the edge impedance equals the resistive part, which allows measurement of resistance down to two orders of magnitude below the transport noise. In the vicinity of the melting transition, we find that once the c -axis contribution is eliminated via ion irradiation of the current contacts, the edge resistance shows no sharp features at melting.

We thank H. Shtrikman for GaAs heterostructures and M. Konczykowski for ion irradiation. This work was supported by the German-Israeli Foundation (GIF). HB acknowledges the support of the Adams Fellowship Program of the Israel Academy of Sciences and Humanities and EZ the US-Israel Binational Science Foundation (BSF).

* Electronic address: haim.beidenkopf@weizmann.ac.il

- [1] G. Blatter *et al.*, *Rev. Mod. Phys.* **66**, 1125 (1994).
- [2] G. P. Mikitik and E. H. Brandt, *Phys. Rev. B* **68**, 054509 (2003).
- [3] E. Zeldov *et al.*, *Nature* **375**, 373 (1995).
- [4] A. Schilling *et al.*, *Phys. Rev. Lett.* **78**, 4833 (1997).
- [5] H. Safar *et al.*, *Phys. Rev. Lett.* **68**, 2672 (1992).
- [6] C. J. van der Beek *et al.*, *Physica C* **195**, 307 (1992).
- [7] H. Beidenkopf *et al.*, *Phys. Rev. Lett.* **95**, 257004 (2005).
- [8] H. Beidenkopf *et al.*, *Phys. Rev. Lett.* **98**, 167004 (2007).
- [9] D. T. Fuchs *et al.*, *Phys. Rev. Lett.* **80**, 4971 (1998).
- [10] E. Forgan, *Czech. J. Phys.* **46**, 1571 (1996).
- [11] T. Shibauchi *et al.*, *Phys. Rev. Lett.* **83**, 1010 (1999).
- [12] Y. Ando and K. Nakamura, *Phys. Rev. B* **59**, R11661 (1999).
- [13] K. Kimura *et al.*, *Physica B* **284**, 717 (2000).

- [14] Y. Eltsev *et al.*, *Physica C* **341**, 1107 (2000).
- [15] R. Sugano *et al.*, *Physica B* **284**, 803 (2000).
- [16] Y. Nonomura and X. Hu, *Phys. Rev. Lett.* **86**, 5140 (2001).
- [17] D. Li, P. Lin and B. Rosenstein, *Physica C* **468**, 1245 (2008).
- [18] J. Dietel and H. Kleinert, *Phys. Rev. B* **79**, 014512 (2009).
- [19] A. V. Samoilov *et al.*, *Phys. Rev. Lett.* **76**, 2798 (1996).
- [20] L. I. Glazman and A. E. Koshelev, *Phys. Rev. B* **43**, 2835 (1991).
- [21] B. Horovitz and T. R. Goldin, *Phys. Rev. Lett.* **80**, 1734 (1998).
- [22] H. M. Carruzzo and C. C. Yu, *Philos. Mag. B* **77**, 1001 (1998).
- [23] E. Frey, D. R. Nelson and D. S. Fisher, *Phys. Rev. B* **49**, 9723 (1994).
- [24] M. Feigel'man, V. Geshkenbein and A. Larkin, *Physica C* **167**, 177 (1990).
- [25] C. P. Bean and J. D. Livingston, *Phys. Rev. Lett.* **12**, 14 (1964).
- [26] E. Zeldov *et al.*, *Phys. Rev. Lett.* **73**, 1428 (1994).
- [27] D. T. Fuchs *et al.*, *Nature* **391**, 373 (1998).
- [28] L. Burlachkov, A. E. Koshelev and V. M. Vinokur, *Phys. Rev. B* **54**, 6750 (1996).
- [29] E. H. Brandt, G. P. Mikitik and E. Zeldov, *Phys. Rev. B* **74**, 094506 (2006).
- [30] C. J. van der Beek and P. H. Kes, *Phys. Rev. B* **43**, 13032 (1991).
- [31] D. G. Steel and J. M. Graybeal, *Phys. Rev. B* **45**, 12643 (1992).
- [32] R. Busch *et al.*, *Phys. Rev. Lett.* **69**, 522 (1992).
- [33] B. Khaykovich *et al.*, *Phys. Rev. B* **61**, R9261 (2000).
- [34] D. R. Nelson and V. M. Vinokur, *Phys. Rev. Lett.* **68**, 2398 (1992).
- [35] M. Konczykowski *et al.*, *Phys. Rev. B* **51**, 3957 (1995).
- [36] T. Tamegai *et al.*, *J. Low Temp. Phys.* **117**, 1363 (1999).
- [37] R. A. Doyle *et al.*, *Phys. Rev. Lett.* **77**, 1155 (1996).
- [38] W. S. Seow *et al.*, *Phys. Rev. B* **53**, 14611 (1996).
- [39] D. T. Fuchs *et al.*, *Phys. Rev. B* **54**, R796 (1996).
- [40] D. T. Fuchs *et al.*, *Phys. Rev. B* **55**, R6156 (1997).
- [41] S. Colson *et al.*, *Phys. Rev. Lett.* **90**, 137002 (2003).